
Article:
Smith, David Kelham orcid.org/0000-0002-9881-2714 (2017) Emergence of highly-ordered hierarchical nanoscale aggregates on electrostatic binding of self-assembled multivalent (SAMul) cationic micelles with polyanionic heparin. Journal of Materials Chemistry B. pp. 341-347. ISSN 2050-750X

https://doi.org/10.1039/c6tb02512a

Journal Name

ARTICLE

Emergence of highly-ordered hierarchical nanoscale aggregates on electrostatic binding of self-assembled multivalent (SAMul) cationic micelles with polyanionic heparin

Received 00th January 20xx,
Accepted 00th January 20xx

DOI: 10.1039/x0xx00000x

www.rsc.org/

Vania M. P. Vieira,[a] Ville Liljeström,[b] Paola Posocco,[c] Erik Laurini,[c] Sabrina Pricl,[c] Mauri A. Kostiainen[b,*] and David K. Smith[a,*]

We report three surfactants, with cationic *N*,*N*-di-(3-aminopropyl)-*N*-methylamine (DAPMA) head groups and aliphatic chains connected via an amide linkage, and investigate their ability to self-assemble and bind polyanionic heparin – a process of potential clinical importance in coagulation control. Modifying the hydrophobic chain length tunes the self-assembly event, with C16-DAPMA having the lowest critical micelle concentration and also being the optimal heparin binder. Remarkably highly structured hierarchical nanoscale aggregates are formed on binding between the spherical cationic micelles and linear polyanionic heparin. C14-DAPMA and C16-DAPMA yield organized polycrystalline assemblies as observed by transmission electron microscopy (TEM), predicted in solution by mesoscale simulations and characterized by small-angle X-ray scattering (SAXS). This confirms that the micelles remain intact during the hierarchical assembly process and become packed in a face-centered cubic manner. The nanoscale assembly formed by C16-DAPMA showed the highest degree of order. Importantly, these studies indicate the impact of hydrophobic modification on self-assembly and heparin binding, demonstrate remarkably high stability of these self-assembled micelles even when forming strong electrostatic interactions with heparin, and provide structural insights into nanoscale hierarchical electrostatic assemblies.

Introduction

Polyanions are ubiquitous in natural systems – from the polynucleotides which control hereditary information to glycosaminoglycans (GAGs) which play vital roles in many biological processes.[1] Binding polyanions is therefore of key importance in biology and a number of proteins have evolved to this task, usually by making use of multiple cationic residues, exploiting electrostatic ion-ion interactions. This binding is relatively non-directional, but can deliver high amounts of binding energy, even in highly competitive media such as water, and can impart surprising levels of selectivity.[2] In more general terms, the use of electrostatic interactions for directed assembly of nanoscale structured materials has recently become an area of considerable importance in nanoscience.[3] The use of multiple binding groups, a 'multivalent' strategy, is a well-known method for enhancing binding between nanoscale surfaces in challenging conditions.[4] For polyanion binding, multivalent cations are usually displayed either on (i) cationic polymers, or (ii) cationic lipids which form polycationic assemblies – these two key strategies are applied in (e.g.) the delivery of polyanionic genetic material.[5]

Heparin is a polyanionic GAG of particular interest owing to its key roles in biological processes such as blood coagulation and angiogenesis – it is used as an anti-coagulant during major surgery and to prevent thrombosis in bed-bound patients.[6] In the case of surgical intervention, it is necessary to reverse the effect of heparin once surgery is complete – there is therefore considerable interest in developing systems which achieve effective heparin reversal.[7] In many cases these heparin binders are polycationic. Our own research has focused on the development of low-molecular-weight building blocks which form self-assembled multivalent (SAMul) heparin binders – such systems have advantages for coagulation control in terms of synthetic simplicity and tunability, high activity as a result of mulltivalent binding and pharmaceutically-useful degradation and disassembly profiles.[8] Given the clinical importance of heparin binding,[9] it is vital to understand the self-assembly and binding mechanisms inherent in this SAMul approach.

As noted above, binding events which take place between oppositely charged polyelectrolytes are the focus of considerable general interest.[10] In particular, the interaction between surfactant micelles and polyelectrolytes has been widely explored and well-reviewed.[11] Such interactions underpin a number of important consumer applications, including systems for targeted storage, delivery and controlled release, with the presence of both polyelectrolyte and oppositely-charged surfactant giving rise to complementary, and sometimes synergistic effects.[12] A number of fundamental

[a] Department of Chemistry, University of York, Heslington, York, YO10 5DD, UK. Email: david.smith@york.ac.uk.
[b] Biohybrid Materials, Department of Biotechnology and Chemical Technology, Aalto University, 00076 Aalto, Finland. Email: mauri.kostiainen@aalto.fi
[c] Simulation Engineering (MOSE) Laboratory, Department of Engineering and Architectures (DEA), University of Trieste, Trieste, 34127, Italy
Electronic Supplementary Information (ESI) available: synthesis and characterisation data, original data from DLS, heparin binding assays. See DOI: 10.1039/x0xx00000x

studies have explored the interactions which underpin this kind of binding, and it is generally understood that counter-ions are displaced from the micelle surface and replaced with the polyelectrolyte.[13] Li and Wagner tried to consolidate many of these studies and reported universal binding behaviour for ionic alkyl surfactants with polyanions, noting the importance of surfactant hydrophobicity and polymer charge density in controlling cooperative binding strength.[14] It has also been noted that flexibility/rigidity can play important roles in polyelectrolyte binding.[15]

With the fundamental interest in this kind of binding process in mind, and also considering the clinical interest in heparin binding for the reversal of anti-coagulation therapy following surgical intervention, we wanted to characterize our SAMul heparin binders in greater structural detail. Although such studies have been performed for DNA binding systems,[5] there is currently no understanding of heparin binding in these terms. The aim of this current study was to investigate a minimal self-assembling system in terms of its heparin-binding ability, and probe the impact of the hydrophobic region on self-assembly and heparin binding. Most importantly, we aimed to characterise the self-assembly and binding events across all length-scales, and for the first time gain insight into the remarkable hierarchical nanoscale assembly processes which take place when these oppositely charged, and differently shaped, polyionic species are brought together.

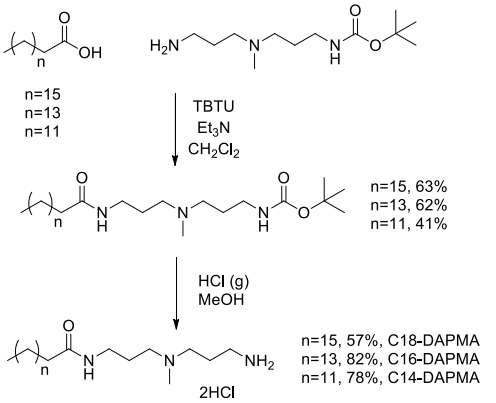

Scheme 1. Synthesis of target surfactants C14-DAPMA, C16-DAPMA and C18-DAPMA investigated in this paper as heparin binding agents.

Results and Discussion

Three simple amphiphilic heparin binders were designed with a polar head group constructed from *N*,*N*-di-(3-aminopropyl)-*N*-methylamine (DAPMA) and an apolar tail constituted by saturated fatty acids with 14, 16 and 18 carbon atoms (myristic acid, palmitic acid and stearic acid respectively). The molecules were constructed using TBTU-mediated peptide coupling with a Boc-protecting group strategy (Scheme 1), yielding C14-DAPMA, C16-DAPMA and C18-DAPMA in good overall yields. We previously reported C16-DAPMA as part of a study of ligand effects on polyanion binding.[8d] In this new study, we wanted to investigate the impact of hydrophobic chain on self-assembly, heparin binding and nanostructuring – it was predicted this should modify polyanion binding,[14] even though the hydrophobic unit is not itself directly involved at the binding interface.

We used a Nile Red assay[16] to determine the critical micelle concentrations (CMCs) of the synthesized amphiphiles in phosphate buffered saline (PBS, 10 mM, Table 1). As expected, C14-DAPMA has the highest CMC value because it has the smallest hydrophobic chain and therefore the lowest driving force for self-assembly. The CMC of C16-DAPMA was significantly lower as the longer chain assists self-assembly. Perhaps surprisingly, however, the CMC value for C18-DAPMA was higher than for C16-DAPMA. We suggest this is a result of the relatively low solubility of C18-DAPMA in PBS buffer caused by the larger hydrophobic block – we have noted for related compounds that the balance between hydrophobic and hydrophilic block size is important in controlling solubility,[8d] as is well-known in surfactant chemistry.[17]

Table 1. CMC values of assemblies formed by C14-DAPMA, C16-DPAMA and C18-DAPMA as assessed by Nile Red assay in PBS buffer (10 mM), and Z-average hydrodynamic diameter and ζ-potential of C14-DAPMA, C16-DAPMA and C18-DAPMA derived by DLS (10 mM Tris-HCl, 150 mM NaCl).

Sample	CMC (μM)	Diameter (nm)	ζ-Potential (mV)
C14-DAPMA	116.5 ± 1.4	5.8 ± 1.6	41.3 ± 1.6
C16-DAPMA	38.5 ± 0.4	6.2 ± 1.3	51.7 ± 2.2
C18-DAPMA	73.0 ± 5.9	93 ± 26	54.1 ± 4.2

To characterise the self-assembled nanostructures in more detail, we employed dynamic light scattering (DLS). The results (Table 1) indicated that C14-DAPMA and C16-DAPMA assembled into micelles with diameters of ca. 5.8 nm and 6.2 nm respectively. These sizes are in agreement with expectations for micelles formed from these surfactants packing without overlap of hydrophobic chains. As expected, the aggregates formed by C16-DAPMA were slightly bigger than those formed by C14-DAPMA, due to the difference in length of the hydrocarbon chain, with C16-DAPMA having two additional carbon-carbon bonds, which results in four additional bonds when the micelles are formed and packed tail-to-tail, hence giving rise to the observed micellar size increase. Interestingly, however, DLS revealed the predominant presence of larger aggregates for C18-DAPMA (ca. 100 nm). It should be noted that DLS is carried out at relatively high concentration, and this can encourage aggregation into larger structures. Clearly, however, C18-DAPMA is more susceptible to this than C14-DAPMA or C16-DAPMA. We suggest this is in-line with the visual observation that the solubility of C18-DAPMA was relatively poor, and propose that a degree of non-specific aggregation occurs as a result of the larger hydrophobic block. High ζ-potentials were obtained for each of the three binders, indicating the existence of highly-charged cationic nanoscale surfaces as a result of protonation of DAPMA at physiological pH values. The ζ-potential becomes larger as the hydrophobic block becomes bigger, presumably because there is a greater driving force for the assembly of positively charged molecular building blocks into close proximity, enabling the formation of micelles with higher surface charge density. Furthermore, the larger size of nanostructures formed by C18-DAPMA may

incorporate a greater total charge and support a greater charge density.

We then went on to perform Mallard Blue (MalB) competition assays to test the heparin binding of each system. In this methodology,[18] the displacement of the dye MalB from its complex with heparin is monitored using UV-Vis spectroscopy. This assay enables the calculation of the charge excess (CE_{50}) corresponding to the number of positive charges needed per heparin negative charge to obtain 50% displacement of MalB, the effective concentration (EC_{50}) of binder at the same point and 'dose', which is the mass of binder required to bind 100 international units (IU, the clinical measurement) of heparin.

All three binders bind heparin and displace MalB at micromolar concentrations, indicative of effective self-assembled multivalent (SAMul) binding (Table 2). Although C18-DAPMA has the highest ζ-potential as determined by DLS, this does not translate into the best binding of polyanionic heparin. Indeed, among the three binders C16-DAPMA had the highest efficiency in terms of MalB displacement and hence heparin binding. This would suggest that in the same way that self-assembly and CMC were optimised for this molecular structure as a result of it possessing the optimal hydrophobic/hydrophilic balance, these optimal self-assembly properties are translated into its heparin binding capability. Nonetheless, all three compounds were effective heparin binders. It should be noted that heparin binding occurs at concentrations below the CMC – this is not surprising as it is well-known that the presence of polyanions can encourage the self-assembly of oppositely-charged polycations, and lower the effective CMC.[19] Furthermore, this provides a mechanism by which optimised self-assembly, as observed for C16-DAPMA, can be matched with heparin binding, as these two processes act to reinforce one another.

Table 2. CE_{50}, EC_{50} and dose values obtained for C14-DAPMA, C16-DAPMA and C18-DAPMA using MalB competition assay (10 mM TrisHCl, 150 mM NaCl, pH 7.0).

Sample	CE_{50}	EC_{50} / μM	Dose / mg 100 IU^{-1}
C14-DAPMA	0.88 ± 0.05	48 ± 3	0.59 ± 0.03
C16-DAPMA	0.64 ± 0.02	34 ± 1	0.46 ± 0.01
C18-DAPMA	0.68 ± 0.09	37 ± 5	0.52 ± 0.07

We then used DLS in an attempt to characterise the complexes formed. When the binders (1 mg/mL) were in the presence of heparin (at 2:1 binder:heparin charge ratio) a significant increase in size was observed (Table 3). The presence of larger aggregates when the binders are in the presence of heparin suggests the formation of agglomerates between the oppositely charged components, providing further evidence of the existence of interactions between the binders and heparin. Furthermore, on binding to heparin, the ζ-potential decreased, as a result of charge neutralisation induced by heparin binding – the charge neutralisation was greatest for the least effective binder C14-DAPMA, while the most effective binder C16-DAPMA, showed the lowest extent of charge neutralisation – in line with the view that C16-DAPMA is actually very efficient in using its positive charge to bind to the fixed amount of heparin present. DLS therefore suggests a degree of nanoscale aggregation between the polycationic self-assembled micelles and heparin polyanions. The evolution of hierarchical structures in micelle-polyelectrolyte systems is a known phenomenon, but has not previously been explored in detail for heparin binding.[20]

Table 3. Average hydrodynamic diameter and ζ-potential of C14-DAPMA, C16-DAPMA and C18-DAPMA in the presence of heparin (Binders: 1 mg/mL. Heparin concentration was calculated using a Binder-Heparin charge ratio of 2:1 resulting in 0.35, 0.37 and 0.39 mg/mL of heparin for C18, C16 and C14, respectively (10 mM Tris-HCl, 150 mM NaCl, pH 7.0).

Sample	Diameter (nm)	ζ–Potential (mV)
C14-DAPMA+Heparin	1321 ± 249	-8.0 ± 0.5
C16-DAPMA+Heparin	1185 ± 151	26.6 ± 0.8
C18-DAPMA+Heparin	480 ± 59	4.8 ± 0.7

To probe this process in more depth, we used DLS to study the impact of the C16-DAPMA:Heparin ratio on hierarchical assembly and aggregation. Table 4 indicates that as the loading of heparin increases (going down the table), the size of the assemblies increases, reflecting increased levels of hierarchical aggregation of the nanoscale micelles formed by C16-DAPMA. Indeed, even very small amounts of heparin (10:1 ratio) lead to significant hierarchical aggregation. Furthermore, the ζ-potential decreases – reflecting charge neutralisation. Aggregates with zero ζ-potential are observed when the nominal charge ratio is ca. 2.25:1 suggesting that not all of the micellar cationic sites within the aggregates need be completely satisfied by binding to an anion on heparin.

Table 4. Average hydrodynamic diameter (measured by volume distribution) and ζ-potential of C16-DAPMA (always 1 mg/mL) in the presence of increasing amounts of heparin (10 mM Tris-HCl, 150 mM NaCl, pH 7.0).

Charge ratio (+:-)	Diameter (nm)	ζ-Potential (mV)
10:1	548 ± 248	43.5 ± 2.4
9:1	700 ± 221	49.1 ± 1.0
8:1	1059 ± 412	43.8 ± 1.5
7:1	1142 ± 326	45.6 ± 1.0
6:1	1064 ± 191	43.3 ± 1.6
5:1	1117 ± 314	40.3 ± 3.3
4:1	1512 ± 224	31.8 ± 4.1
3:1	1422 ± 198	26.5 ± 4.7
2:1	1730 ± 448	-11.5 ± 0.1
1:1	1486 ± 220	-23.5 ± 0.7

To gain greater further insight into the morphologies of the self-assembled micelles and the way in which they aggregate in the presence of heparin, we performed transmission electron microscopy (TEM). TEM images were obtained for each of the three binders before and after binding to heparin. It should be noted that TEM imaging is performed on dried samples, and as such, the drying step may give rise to some morphological change. Compounds C14-DAPMA and C16-DAPMA both formed spherical self-assembled nanostructures (Fig. 1a,b, left), in agreement with DLS. Remarkably, on binding to heparin, these systems formed highly-organised semi-crystalline

nanostructured arrays (Fig. 1a,b, right). We have observed related structural effects before on binding between micelles and heparin, but the examples reported here have particularly high levels of structural definition and order. We reasoned that a hierarchical nanoscale self-assembly process is taking place between the spherical cationic micelles, and the 'linear' heparin polyanions (see below for detailed analysis). These TEM observations clearly suggest that the self-assembled micelles formed by C14-DAPMA and C16-DAPMA have excellent stability, and appear to remain intact without disruption or reorganisation, even in the presence of heparin, with which they can form very strong electrostatic interactions. The diameters of the micelles observed by TEM on assembly with heparin are in good agreement with the micellar diameters observed by DLS (see below for detailed analysis).

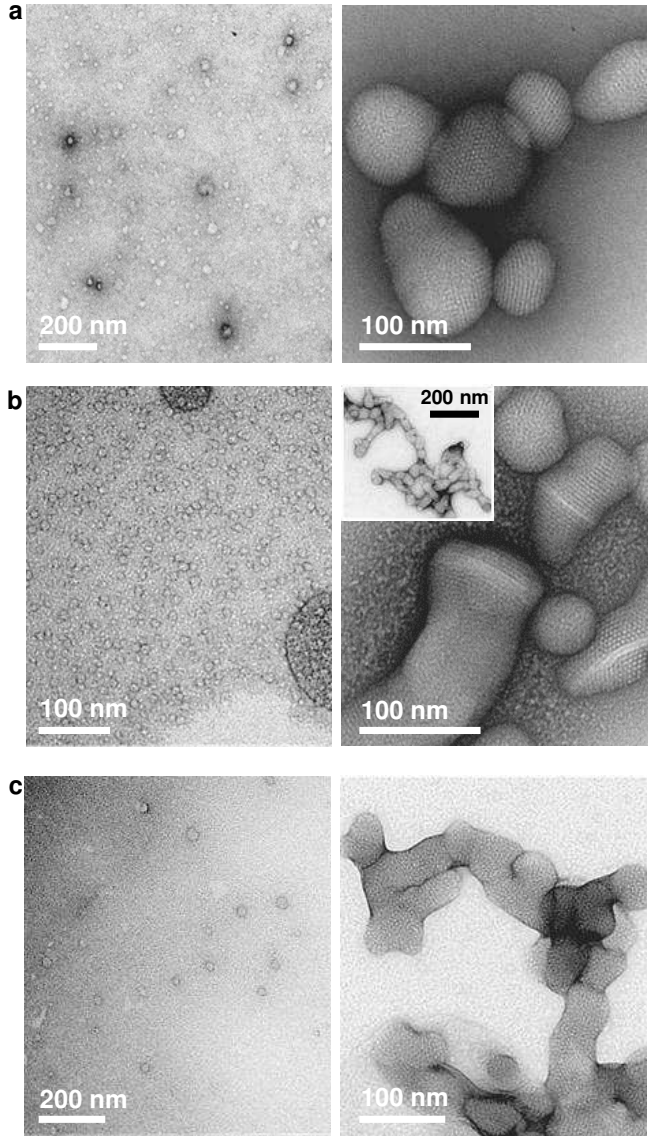

Figure 1. TEM images of (a) C14-DAPMA (left) and C14-DAPMA with heparin (right); (b) C16-DAPMA (left) and C16-DAPMA with heparin (right); (c) C18-DAPMA (left) and C18-DAPMA with heparin (right).

C18-DAPMA particles did not form such obvious well-defined small spherical micelles (Fig. 1c, left), and although aggregation was still observed on heparin binding, this appeared to be somewhat less ordered (Fig. 1c, right) in terms of hierarchical structuring. This is in-line with the DLS observations which suggested that the self-assembly of this compound is less well-defined, presumably as a consequence of its lower solubility and a greater tendency to aggregate in an uncontrolled way – especially at elevated concentrations.

Given the potential clinical relevance of self-assembled nanostructures for heparin binding and reversal,[9] we considered it of great importance to verify whether the highly ordered hierarchical nanoscale aggregates revealed by TEM for C14-DAPMA and C16-DAPMA are preserved in solution. To the purpose, Dissipative Particle Dynamics (DPD) simulations[8,15b,18] were initially employed to predict the self-assembly and spatial organization of these two amphiphiles in solution in presence of heparin (Figure 2).

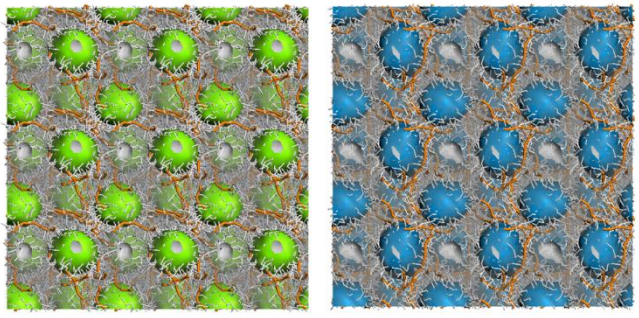

Figure 2. DPD snapshots of C14-DAPMA (left) and C16-DAPMA (right) self-assembly in presence of heparin (2:1 binder:heparin ratio). The hydrophobic micellar core is highlighted as green and blue isosurfaces, respectively. Hydrophilic moieties of each aggregate are shown as white sticks, while heparin molecules are visualized as orange rods. A continuous light grey field portrays the aqueous medium.

In agreement with TEM analysis, mesoscale computational models reveal that both binders self-assemble into highly ordered spherical nanostructures which remain intact in the presence of the polyanion. In both cases, the nanoscale organization is characterized by face-centred cubic (fcc) packing of the hierarchical assemblies, as evidenced by the relevant isodensity surfaces of the micellar hydrophobic cores (Figure 2). The predicted lattice structures of C14-DAPMA and C16-DAPMA micelle are characterized by lattice constants, *a*, of 8.1 nm and 8.6 nm, respectively. Thus, the unit cell size of the fcc structure of C16-DAPMA is predicted to be slightly bigger than that of C14-DAPMA. The corresponding centre-to-centre distance ($a/\sqrt{2}$) is 5.7 nm for C14-DAPMA and 6.1 nm for C16-DAPMA – in good agreement with the micelle diameters reported from DLS.

Next, the nanostructure of the aqueous binder-heparin complex was investigated by small angle X-ray scattering (SAXS) for C14-DAPMA and C16-DAPMA. The obtained 2D diffraction patterns (Fig. 3a inset) show, for both binder-heparin complexes, a Debye ring with a diffuse symmetric halo that does not present intensity differences, which is typical for polycrystalline samples with isotropic orientation of multiple crystals.[21] For the assembly formed between C14-DAPMA and

heparin the positions of the diffraction peaks were at q = 0.129 and 0.259 Å^{-1} which in terms of crystal plane reflections with Miller indices corresponds to (*hkl*) = (111) and (222), assuming a face-centred cubic (fcc) structure. For the assemblies comprising C16-DAPMA and heparin, SAXS measurements (Fig. 3a) showed diffraction peaks at q = 0.122, 0.138 and 0.246 Å^{-1} which in terms of crystal plane reflections with Miller indices corresponds to (*hkl*) = (111), (200) and (222), assuming a fcc structure. The additional observation of the (200) peak for the C16-DAPMA complexes, not observed for those formed by C14-DAPMA, may be suggestive of a greater degree of nanocrystalline order for the C16-DAPMA system or a different form factor for the micelles. This would be in agreement with the lower CMC and greater heparin binding ability observed for this compound, as well as the very highly ordered repetitive structures observed by TEM.

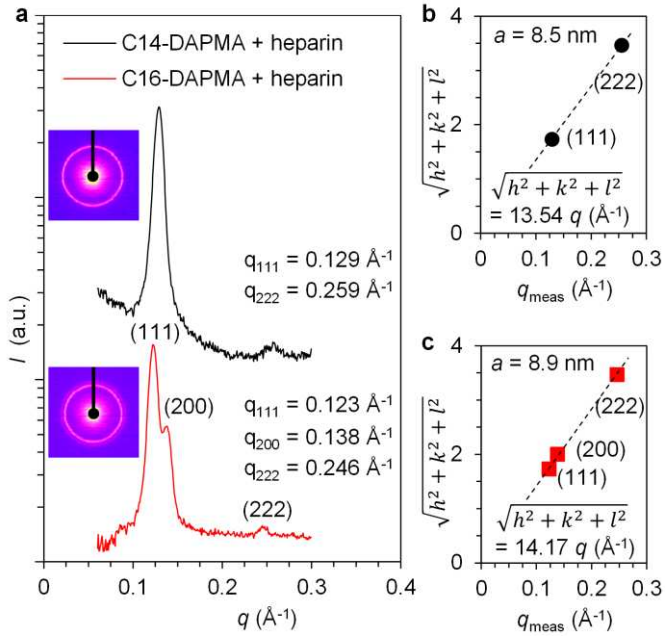

Figure 3. SAXS characterization of C14-DAPMA and C16-DAPMA in the presence of heparin. (a) Integrated SAXS curve measured from self-assembled C14-DAPMA and C16-DAPMA in the presence of heparin. Inset: 2D-scattering pattern of C14-DAPMA and C16-DAPMA with heparin. Quadratic Miller indices of assigned reflections for fcc structure versus measured q-vector positions for indexed peaks, related with (b) C14-DAPMA binding heparin and (c) C16-DAPMA binding heparin.

It has been noted that in the same way atomic structure controls crystallisation events, molecular structures can play a directing role in the formation of nanocrystalline assemblies via electrostatic interactions between polyionic species.[22] In this case, the modification of lattice parameters based on the size of the molecular scale surfactant building block is a clear example of the way in which molecular parameters can be translated into the packing of hierarchical nanocrystalline structures.

The quadratic Miller indices were plotted against the measured $q_{(hkl)}$ values for C14-DAPMA-heparin and C16-DAPMA-heparin complexes, as shown in Figure 3b and c, respectively. The lattice constant a, was then estimated by linear regression. For cubic phases $a = 2\pi\sqrt{(h^2+k^2+l^2)}/q_{(hkl)}$, which was determined to be 8.5 nm for C14-DAPMA and 8.9 nm for C16-DAPMA, in good agreement with the corresponding values obtained from the theoretical calculations. The centre-to-centre distance ($a/\sqrt{2}$) of the particles was 6.0 nm for the C14-DAPMA and 6.3 nm for the C16-DAPMA, again in line with mesoscale predictions.

The centre-to-centre distances are also in very good agreement indeed with the micellar diameters determined by DLS methods. It should be remembered that DLS is a solution-phase method which also includes the solvent and counterions at the micellar periphery, which will be replaced by polyanion once heparin has bound. As such, and supported by the binder:heparin complex organization predicted by simulation, these SAXS data would fit with a view in which self-assembled cationic micelles are packed into a polycrystalline array by polyanionic heparin in analogy to the ionic model. Most importantly, these SAXS results confirm that the self-assembled micelles retain their structural integrity on binding to heparin, and are not disrupted, even on formation of high-affinity electrostatic interactions with their binding partner.

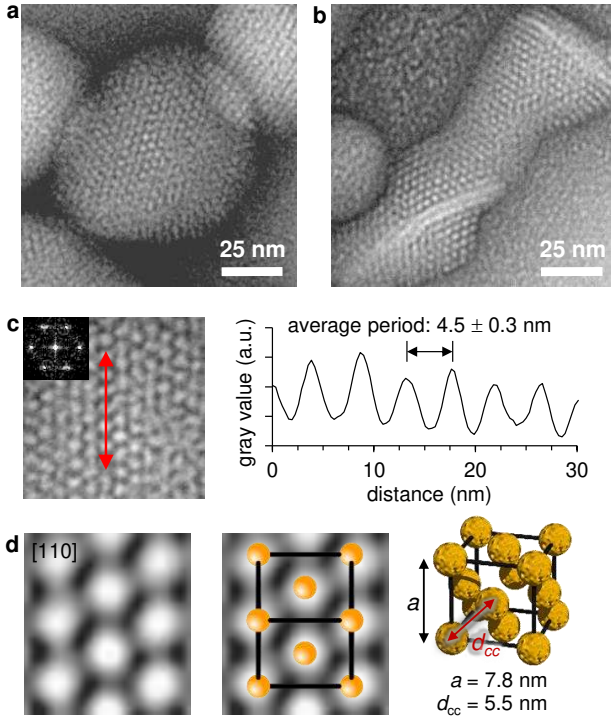

Figure 4. TEM images of C14-DAPMA (a) and C16-DAPMA (b) heparin complex. (c) A crystalline area for C14-DAPMA (left, inset: fast Fourier transform) and a line profile analysis (right) along the red line. (d) Filtered inverse Fourier transform from selected Fourier components for C14-DAPMA (left), overlay of the image and fcc unit cell (middle) and model of the fcc unit cell with key dimension (right). Micelles shown in yellow, diameter reduced for clarity.

Finally, the data obtained from simulations and SAXS were compared with the TEM images. Figure 4 shows the TEM images of (a) C14-DAPMA and (b) C16-DAPMA binding to heparin. For C14-DAPMA, Figure 4 illustrates the crystal projection viewed along the [110] zone axis (c, left). Analysing the line profile over the crystal projection (marked in red) yields an average period (ap) of 4.5 ± 0.3 nm, which corresponds to a fcc lattice constant (a = 3ap/$\sqrt{3}$) of 7.8 ± 0.5 nm for C14-DAPMA. As expected, the corresponding values for C16-DAPMA are slightly higher (ap = 4.6 ± 0.3 nm and a = 8.0 ± 0.5 nm, see ESI for the Figures associated with C16-DAPMA). These values are in very good agreement indeed with the a values obtained by DPD and SAXS

– the slight reduction in the unit cell size can be attributed to a drying effect on the TEM grid. Calculating a fast Fourier transform (Figure 4c inset) from the crystalline area (Figure 4c) and filtering the inverse Fourier transform from selected Fourier components, yields an image that represents the unit cell of the crystal viewed along the [110] zone axis (Figure 4d, left). This can be also confirmed by overlaying the image and a model of the unit cell (Figure 4d, middle) shown in Figure 4d, right. The centre-to-centre distances of 5.5 nm and 5.6 nm for C14-DAPMA and C16-DAPMA respectively are in very good agreement with the micelle diameters from DLS and the corresponding centre-to-centre distances from DPD and SAXS. Taken together, therefore, our data indicates that the proposed hierarchical nanoscale assembly model is valid, and confirms the viewpoint that the micellar objects have excellent structural integrity and can be considered as intact nanoscale building blocks throughout the heparin binding and hierarchical assembly process.

Conclusions

In summary, we have reported a family of simple self-assembling surfactant molecules and investigated their ability to bind heparin. Modifying the hydrophobic chain length offers a mechanism for tuning the ability of these compounds to self-assemble into micellar aggregates, with C16-DAPMA being the optimal system in terms of CMC. Furthermore, this compound is also the most effective heparin binder as determined by MalB displacement assays – we suggest this indicates the synergy between surfactant self-assembly and polyanion binding. For the first time, we have structurally characterized the nanoscale aggregates formed on binding between SAMul cationic spherical micelles, and polyanionic cylindrical heparin. In particular, C14-DAPMA and C16-DAPMA formed highly organised nanocrystalline assemblies as observed by TEM. Characterization by mesoscale simulations and SAXS further confirmed that the micelles remained intact during hierarchical assembly and were packed in a face-centred cubic manner on contact with heparin. The assemblies formed by the most effective system, C16-DAPMA showed the highest degree of crystalline order revealed by the distinct diffraction peaks. Dimensions could be directly correlated between DLS, TEM, simulations and SAXS, indicative of the high stability of these self-assembled micelles even when they form very strong electrostatic interactions with heparin, indicating they can be considered as distinct building blocks for nanoscale assembly even in very competitive conditions.

Acknowledgements

This research was supported by Marie Curie ITN Funding as part of the project 'SMART-NET' (Early Stage Researcher funding to VMPV). Financial support from Academy of Finland (projects 263504, 267497, 273645, 286845) and Biocentrum Helsinki is gratefully acknowledged. This work was carried out under the Academy of Finland's Centers of Excellence Programme (2014–2019) and made use of Aalto University Nanomicroscopy Center.

Notes and references

1 L. S. Jones, B. Yazzie and C. R. Middaugh, *Mol. Cell. Proteomics*, 2004, **3**, 746-769.

2 (*a*) I. Capila and R. J. Linhardt, *Angew. Chem. Int. Ed.*, 2002, **41**, 391-412. (*b*) M. C. Z. Meneghetti, A. J. Hughes, T. R. Rudd, H. B. Nader, A. K. Powell, E. A. Yates and M. A. Lima, *J. Roy. Soc. Interface*, 2015, **12**, 20150589.

3 D. A. Walker, B. Kowalczyk, M. O. de la Cruz and B. A. Grzybowski, *Nanoscale*, 2011, **3**, 1316-1344.

4 (*a*) C. Fasting, C. A. Schalley, M. Weber, O. Seitz, S. Hecht, B. Koksch, J. Dernedde, C. Graf, E. W. Knapp and R. Haag, *Angew. Chem. Int. Ed.*, 2012, **51**, 10472-10498. (*b*) A. Barnard and D. K. Smith, *Angew. Chem. Int. Ed.*, 2012, **51**, 6572-6581.

5 (*a*) R. Srinivas, S. Samanta and A. Chaudhuri, *Chem. Soc. Rev.*, 2009, **38**, 3326-3338. (*b*) A. Aied, U. Greiser, A. Pandit and W. Wang, *Drug Discov. Today*, 2013, **18**, 1090-1098. (*c*) E. Junquera and E. Aicart, *Adv. Colloid Interface Sci.*, 2016, **233**, 161-175.

6 (*a*) R. Barbucci, A. Magnani, S. Lamponi and A. Albanese, *Polym. Adv. Technol.*, 1996, **7**, 675-685. (*b*) D. L. Rabenstein, *Nat. Prod. Rep.*, 2002, **19**, 312-331. (*c*) S. Middeldorp, *Thromb. Res.*, 2008, **122**, 753-762.

7 (*a*) T. W. Wakefield, P. C. Andrews, S. K. Wrobleski, A. M. Kadell, A. Fazzalari, B. J. Nichol, T. Van der Kooi and J. C. Stanley, *J. Surgical Res.*, 1994, **56**, 586-593. (*b*) M. Kikura, M. K. Lee and J. H. Levy, *Anesth. Analg.*, 1996, **83**, 223-227. (*c*) B. P. Schick, D. Maslow, A. Moshinski and J. D. San Antonio, *Blood*, 2004, **103**, 1356-1361. (*d*) S. Choi, D. J. Clements, V. Pophristic, I. Ivanov, S. Vemparala, J. S. Bennett, M. L. Klein, J. D. Winkler and W. F. DeGrado, *Angew. Chem. Int. Ed.*, 2005, **44**, 6685-6689. (*e*) F. Cunsolo, G. M. L. Consoli, C. Geraci and T. Mecca, *US Patent* WO/2005/028422. (*f*) T. Mecca, G. M. L. Consoli, C. Geraci, R. La Spina and F. Cunsolo, *Org. Biomol. Chem.* 2006, **4**, 3763-3768. (*g*) M. Schuksz, M. M. Fuster, J. R. Brown, B. E. Crawford, D. P. Ditto, R. Lawrence, C. A. Glass, L. Wang, Y. Tor and J. D. Esko, *Proc. Natl. Acad. Sci. USA*, 2008, **105**, 13075-13080. (*h*) R. E. McAllister, *Circulation*, 2010, **122**, A17322. (*i*) J. Kuziej, E. Litinas, D. A. Hoppensteadt, D. Liu, J. M. Walenga, J. Fareed and W. Jeske, *Clin. Appl. Thromb. Hemost.*, 2010, **16**, 377-386. (*j*) G. L. Montalvo, Y. Zhang, T. M. Young, M. J. Costanzo, K. B. Freeman, J. Wang, D. J. Clements, E. Magavern, R. W. Kavash, R. W. Scott, D. H. Liu and W. F. DeGrado, *ACS Chem. Biol.*, 2014, **9**, 967-975. (*k*) R. A. Shenoi, M. T. Kalathottukaren, R. J. Travers, B. F. L. Lai, A. L. Creagh, D. Lange, K. Yu, M. Weinhart, B. H. Chew, C. Du, D. E. Brooks, C. J. Carter, J. H. Morrissey, C. A. Haynes and J. N. Kizhakkedathu, *Science Trans. Med.* 2014, **6**, 260ra150.

8 (*a*) A. C. Rodrigo, A. Barnard, J. Cooper and D. K. Smith, *Angew. Chem. Int. Ed.*, 2011, **50**, 4675-4679. (*b*) S. M. Bromfield, P. Posocco, C. W. Chan, M. Calderon, S. E. Guimond, J. E. Turnbull, S. Pricl and D. K. Smith, *Chem. Sci.*, 2014, **5**, 1484-1492. (*c*) S. M. Bromfield and D. K. Smith, *J. Am. Chem. Soc.*, 2015, **137**, 10056-10059. (*d*) L. E. Fechner, B. Albanyan, V. M. P. Vieira, E. Laurini, P. Posocco, S. Pricl and D. K. Smith, *Chem. Sci.* 2016, **7,** 4653-4659.

9 S. M. Bromfield, E. Wilde and D. K. Smith, *Chem. Soc. Rev.*, 2013, **42**, 9184-9195.

10 (*a*) R. M. Fuoss and H. Sadek *Science*, 1949, **110**, 552-554. (*b*) A. S. Michaels and R. G. Miekka, *J. Phys. Chem.* 1961, **65**, 1765-1773. (*c*) D. V, Pergushov, A. H. E. Muller and F. H. Schacher, *Chem. Soc. Rev.* 2012, **41**, 6886-6901. (*d*) M. Siyawamwaya, Y. E. Choonara, D. Bijukumar, P. Kumar, L. C. Du Toit and V. A.

Pillay, *Int. J. Polym. Mater. Polym. Biomater.* 2015, **64**, 955-968.
11 (*a*) K. Kogej, *Adv. Colloid Interface Sci.* 2010, **158**, 68-83. (*b*) E. Kizilay, A. B. Kayitmazer and P. L. Dubin, *Adv. Colloid Interface Sci*. 2011, **167**, 24-37. (*c*) L. Piculell, *Langmuir*, 2013, **29**, 10313-10329.
12 B. Lindman, F. Antunes, S. Aidarova, M. Miguel and T. Nylander, *Coll. J.* 2014, **76**, 585-594.
13 (*a*) T. Wallin and P. Linse, *Langmuir* 1996, **12**, 305-314. (*b*) T. Wallin and P. Linse, *J. Phys. Chem.* 1996, **100**, 17873-17880. (*c*) P. Hanson, *Langmuir*, 2001, **17**, 4167-4180. (*d*) A. Laguecir, S. Stoll and P. L. Dubin, *J. Phys. Chem. B*, 2003, **107**, 8056-8065.
14 D. Li and N. J. Wagner, *J. Am. Chem. Soc.* 2013, **135**, 17547-17555.
15 (*a*) M. Ram-On, Y. Cohen and Y. Talmon, *J. Phys. Chem. B*, 2016, **120**. 5907-5915. (*b*) S. M. Bromfield, P. Posocco, M. Fermeglia, J. Tolosa, A. Herreros-López, S. Pricl, J. Rodriguez-López and D. K. Smith, *Chem. Eur. J.*, 2014, **20**, 9666-9674
16 M. C. A. Stuart, J. C. van de Pas and J. B. F. N. Engberts, *J. Phys. Org. Chem.,* 2005, **18**, 929-934
17 K. Esumi and M. Ueno, *Structure-Performance Relationships in Surfactants*, Marcel Dekker, New York, 2003
18 (*a*) S. M. Bromfield, A. Barnard, P. Posocco, M. Fermeglia, S. Pricl and D. K. Smith, *J. Am. Chem. Soc.*, 2013, **135**, 2911-2914. (*b*) S. M. Bromfield, P. Posocco, M. Fermeglia, S. Pricl, J. Rodríguez-López and D. K. Smith, *Chem. Commun.*, 2013, **49**, 4830-4832.
19 (*a*) A. J. Konop and R. H. Colby, *Langmuir*, 1999, **15**, 58-65. (*b*) H. Schiessel, M. D. Correa-Rodriguez, S. Rudiuk, D. Baigl and K. Yoshikawa, *Soft Matter*, 2012, **8**, 9406-9411.
20 (*a*) E. Kizilay, A. D. Dinsmore, D. A. Hoagland, L. Sun and P. L. Dubin, *Soft Matter* 2013, **9**, 7320-7332. (*b*) J. E. Laaser, Y. Jiang, S. R. Petersen, T. M. Reineke and T. P. Lodge, *J. Phys. Chem. B* 2015, **119**, 15919-15928.
21 Terentjev, E. M. and Weitz, D. A. (Eds.) *The Oxford Handbook of Soft Condensed Matter*, pp 297-331, 2015
22 (*a*) V. Liljeström, J. Seitsonen and M. A. Kostiainen, *Nature Commun.* 2014, **5**, 4445. (*b*) V. Liljeström, J. Seitsonen and M. A. Kostiainen, *ACS Nano*, 2015, **9**, 11278-11285. (*c*) J. Mikkilä, E. Anaya-Plaza, V. Liljeström, J. R. Caston, T. Torres, A. de la Escosura and M. A. Kostiainen, *ACS Nano*, 2016, **10**, 1565-1571.

Journal Name

ARTICLE

Emergence of highly-ordered hierarchical nanoscale aggregates on electrostatic binding of self-assembled multivalent (SAMul) cationic micelles with polyanionic heparin

Graphical abstract

Self-assembled polycationic micelles can have high levels of structural integrity and form well-defined, structurally ordered hierarchical nanoscale aggregates on interaction with polyanionic heparin in solution.